Bioorganic Chemistry 150 (2024) 107549

Contents lists available at ScienceDirect

Bioorganic Chemistry

journal homepage: www.elsevier.com/locate/bioorg

Stable ubiquitin conjugation for biological interrogation of ubiquitinated tau repeat domain

Giovanna Viola [a], Daniele Trivellato [a], Lorenzo Meulli [b], Roberto Tira [a], Angela Lauriola [a], Francesca Munari [a], Martina Montagnana [c], Mario Buffelli [b], Michael Assfalg [a], Mariapina D'Onofrio [a,*]

[a] Department of Biotechnology, University of Verona, 37134 Verona, Italy
[b] Department of Neurosciences, Biomedicine and Movement Sciences, University of Verona, 37134 Verona, Italy
[c] Department of Engineering for Innovation Medicine, University of Verona, 37134 Verona, Italy

ARTICLE INFO

Keywords:
Tau protein
Ubiquitination
Chemoselective ligation
Dehydroalanine chemistry
Chemical stability
Protein aggregation
Post-translational modifications
Neurodegeneration

ABSTRACT

Protein semisynthesis approaches are key for gaining insights into the effects of post-translational modifications (PTMs) on the structure and function of modified proteins. Among PTMs, ubiquitination involves the conjugation of a small protein modifier to a substrate amino acid residue and is unique in controlling a variety of cellular processes. Interest has grown in understanding the role of ubiquitination in neurodegenerative conditions, including tauopathies. The latter are characterized by the accumulation of the intrinsically disordered protein tau in the form of neurofibrillary tangles in the brains of patients. The presence of ubiquitinated tau in the pathological aggregates suggests that ubiquitination might play a role in the formation of abnormal protein deposits. In this study, we developed a new strategy, based on dehydroalanine chemistry, to install wild type ubiquitin on a tau repeat domain construct with site-specificity. We optimized a three-step reaction which yielded a good amount of highly pure tau repeat domain ubiquitinated in position 353. The structural features of the conjugate were examined by circular dichroism and NMR spectroscopy. The ubiquitinated tau was challenged in a number of assays: fibrils formation under aggregating conditions in vitro, chemical stability upon exposure to a variety of biological media including cell extracts, and internalization into astrocytes. The results demonstrated the wide applicability of the new semisynthetic strategy for the investigation of ubiquitinated substrates *in vitro* or *in cell*, and in particular for studying if ubiquitination has a role in the molecular mechanisms that underlie the aberrant transition of tau into pathological aggregates.

1. Introduction

A hallmark of many neurodegenerative diseases is the slow accumulation of misfolded protein deposits in the neurons of the brain [1]. The microtubule-associated protein tau forms pathological aggregates with the properties of amyloid fibrils in a number of neurodegenerative disorders termed tauopathies, including Alzheimer's disease (AD) and frontotemporal dementia [2]. Tau is an intrinsically disordered protein (IDP) with little propensity for self-aggregation in solution, however in pathological conditions it readily assembles into ordered β-sheet-containing supramolecular filaments [3]. The determinants of abnormal protein aggregation are still poorly understood but the process appears to be strongly influenced by post-translational modifications (PTMs) [4–8].

The greatest research focus has been on the role of hyperphosphorylation in the development of tau pathology. Phosphorylation modulates the interaction of tau with microtubules, and the number and the pattern of the modified sites strongly influence tau structure and aggregation propensity [9]. Another PTM, acetylation, has been shown to regulate tau function, alone or in combination with phosphorylation

Abbreviation: AD, Alzheimer's disease; CD, circular dichroism; CHIP, carboxyl terminus of Hsp70 interacting protein; Dha, Dehydroalanine; DTNB 5, 5 dithio-bis-(2-nitrobenzoic acid); DTT, dithiothreitol; HSQC, Heteronuclear single quantum coherence; IDP, intrinsically disordered protein; MDBP, methyl 2,5-dibromopentanoate; NMR, nuclear magnetic resonance; PTMs, post-translational modifications; SD, standard deviation; TEM, transmission electron microscopy; ThT, Thioflavin-T; Ub, ubiquitin.

* Corresponding author.
E-mail address: mariapina.donofrio@univr.it (M. D'Onofrio).

https://doi.org/10.1016/j.bioorg.2024.107549
Received 17 April 2024; Received in revised form 29 May 2024; Accepted 7 June 2024
Available online 13 June 2024

[10], driving the formation of isoform-specific tau deposits characteristic of different tauopathies [11].

Among the PTMs that decorate tau protein, ubiquitination is by far the least characterized [9]. Ubiquitination (or ubiquitylation) involves the formation of an isopeptide bond between the C-terminal carboxyl group of the small regulatory protein ubiquitin (Ub) and the ε-amino group of lysine sidechains of the protein substrate. The conjugated Ub molecule can be further modified by additional Ub molecules to form elongated chains with diverse linkage topology that elicit different signals [12]. The role of ubiquitination in tau biology and pathology is poorly understood but it has been associated with enhanced formation and impaired clearance of pathological inclusions [13,14]. Alterations to the levels of ubiquitination of tau at various stages of disease have been observed in AD and other tauopathies [15]. The full-length tau isoform (441 amino acids, Fig. S1) has 44 lysine residues, of which 17 were reported as ubiquitination sites, specific to pathological tau [15,16]. The large majority of these sites are in the microtubule binding domain (MBD), which forms the core of the filaments [3,15]. Recent research suggests that ubiquitination, together with other PTMs, may play a role in the structural diversity of various tau strains [5].

Understanding the influence of ubiquitination on the conformational transitions of tau requires a detailed investigation of ubiquitinated proteoforms obtained from controlled reactions. We have previously demonstrated that tau can be ubiquitinated *in vitro* by an enzymatic method, using CHIP (carboxyl terminus of Hsp70 interacting protein) as the ubiquitin ligase (E3) in a chaperone-independent manner [17–19]. This approach affords facile and quantitative mono-ubiquitination of the substrate, however the product is a mixture of regioisomers and is therefore unsuitable for establishing precise structure–function relationships. To overcome this limitation, methods based on chemical synthesis and semisynthesis offer an interesting alternative. A number of elegant chemical approaches have been developed to generate native or non-native linkages between a ubiquitin moiety and a target protein [20,21]. Native chemical ligation [22], often in combination with solid-phase peptide synthesis, has been employed to obtain homogenous ubiquitinated histone [23,24], or α-synuclein [25], and ubiquitin dimers [26]. Silver-mediated chemical modification has been combined with genetic code expansion to generate linkage-specific ubiquitin dimers, allowing the structural characterization and the profiling of the specificity of deubiquitinating enzymes [27,28]. Protein ubiquitination through non-native isopeptide linkage can be achieved using disulfide-directed reactions [29,30], azide-alkyne cycloaddition [20], thiol-ene coupling [31], or thiol-Michael addition [32]. These approaches are often characterized by high reaction rates, efficiency, and good yields.

To study the impact of ubiquitination on the formation of toxic tau species, we first chose an approach based on disulfide coupling chemistry [17,33,34]. This semisynthetic method generates a mimic of the native isopeptide bond, i.e. a disulfide bond between a Cys residue inserted in a specific position of the target protein and the C-terminal aminoethanethiol of a Ub derivative obtained from intein processing [29,35]. Disulfide-based coupling is advantageous as it is regio- and chemoselective, however the resulting product may prove unstable in a weakly reducing environment such as can be found in a living cell. Hence, in the present work, we explored a further strategy for the site-selective ubiquitination of tau through stable covalent conjugation and optimized a method based on dehydroalanine chemistry and thia-Michael addition [32].

Dehydroalanine (Dha) chemistry has been widely exploited for the precise positioning of labels and post-translational modifications on protein substrates [36]. The noncanonical amino acid Dha can be installed at a desired position by diverse methods [37], and sulfur-containing nucleophiles can readily attack the β-carbon atom of Dha to afford a highly selective thia-Michael adduct [32,36]. The reaction can proceed in mild conditions to form a stable thioether linkage. Recent investigations demonstrated the successful application of Dha chemistry for the site-specific phosphorylation and methylation of tau [38,39], and for the ubiquitination of a folded protein substrate [32]. Herein, we describe an optimized chemical mutagenesis protocol for preparing pure Ub conjugates of tau repeat domain (tau4RD) via the Dha precursor, at a specific site. The ubiquitinated tau4RD product was found to exhibit long-term stability in biological media and cell cultures, and a good level of uptake by astrocytes. Thus, the here developed approach provides the basis for an in-depth examination of tau proteoforms, ubiquitinated in a site-specific manner, in biological contexts, enabling a better understanding of structure-(mis)function relationships and assessment of the pathological relevance of the distinct tau species.

2. Results and discussion

2.1. Synthesis of a ubiquitin tau4RD conjugate via dehydroalanine chemistry

For this study, we focused on a construct of tau spanning residues Q244-E372, hereafter tau4RD (Fig. S1). Tau4RD is constituted by the microtubule binding region where most ubiquitination sites are found [15]. Among the different modified positions found *in vivo*, we decided to produce tau ubiquitinated in position 353 in the R4 repeat (Fig. S1). This site was found ubiquitinated in pathological aggregates of tau from AD brains, suggesting a possible role in early events of disease [40], and ubiquitination at this position does not abolish the formation of fibrils in vitro [17,33]. Hence, we believe that investigating the effect of ubiquitination at this site can add further insight into tau pathology. To achieve site-specific installation of a ubiquitin moiety, we designed a semisynthetic strategy based on Dha chemistry. First, we mutated the two native cysteine residues (Cys291, Cys322) of tau4RD into Ala (obtaining cysteine-free tau4RD$^{\Delta C}$), then we introduced a non-native cysteine in the desired position (tau4RD$^{\Delta C}$(353Cys), **I**) using site-directed mutagenesis. Among the possible protocols to introduce Dha, we chose to transform the non-native Cys353 into Dha (tau4RD$^{\Delta C}$(353Dha), **II**) via bis-alkylation elimination using methyl 2,5-dibromopentanoate (MDBP) (Scheme 1-1a) which has been successfully used on tau protein [38,39]. Dha was quantitatively introduced after incubating the reactants for 6 h at 37 °C.

Next, following the intein-mediated ligation approach [41–43], we prepared a thiol-terminated Ub derivative (Ub-SH, **III**) by expression of a Ub-intein fusion protein, followed by cysteamine-mediated cleavage of Ub from intein (Scheme 1-1b). The aminoethanethiol moiety becomes linked to the C-terminus of Ub via *trans*-thioesterification and S,N acyl shift reaction. This approach can produce a full-length wild-type thiol-Ub derivative in high yield for use in the subsequent reaction step. Finally, Ub-SH was conjugated to precursor **II** via 1,4 thia-Michael addition (Scheme 1-2) [32,36], producing homogeneous tau4RD$^{\Delta C}$(353)-S-Ub (hereafter tau4RD(353)-S-Ub, **IV**) with a thioether linkage. Proteoform **IV** contains wild-type ubiquitin and a close mimic of the native conjugate, where the γ-carbon of the lysine sidechain is replaced by sulfur. The progress of the reaction was followed by SDS-PAGE analysis (Fig. 1A). The product **IV** was then purified by HPLC using a gradient of H_2O/acetonitrile (Fig. 1B-C), and the identity of the conjugate and of the reaction intermediates was confirmed by mass spectrometry (Fig. 2). The yield of the reaction was 15 % (purified product). The described method can be easily adapted to obtain tauFL-S-Ub, starting from a tauFL construct (Fig. S1) bearing mutations of the two native cysteine residues (Cys291, Cys322) into alanine (to obtain cysteine-free tauFL$^{\Delta C}$), and introducing a non-native cysteine in the desired position along the entire protein sequence, using site-directed mutagenesis.

2.2. Structural characterization

The intrinsically disordered state of tau is best described as an ensemble of rapidly interconverting conformers with no permanent global or local structural ordering [44]. Short elements of secondary

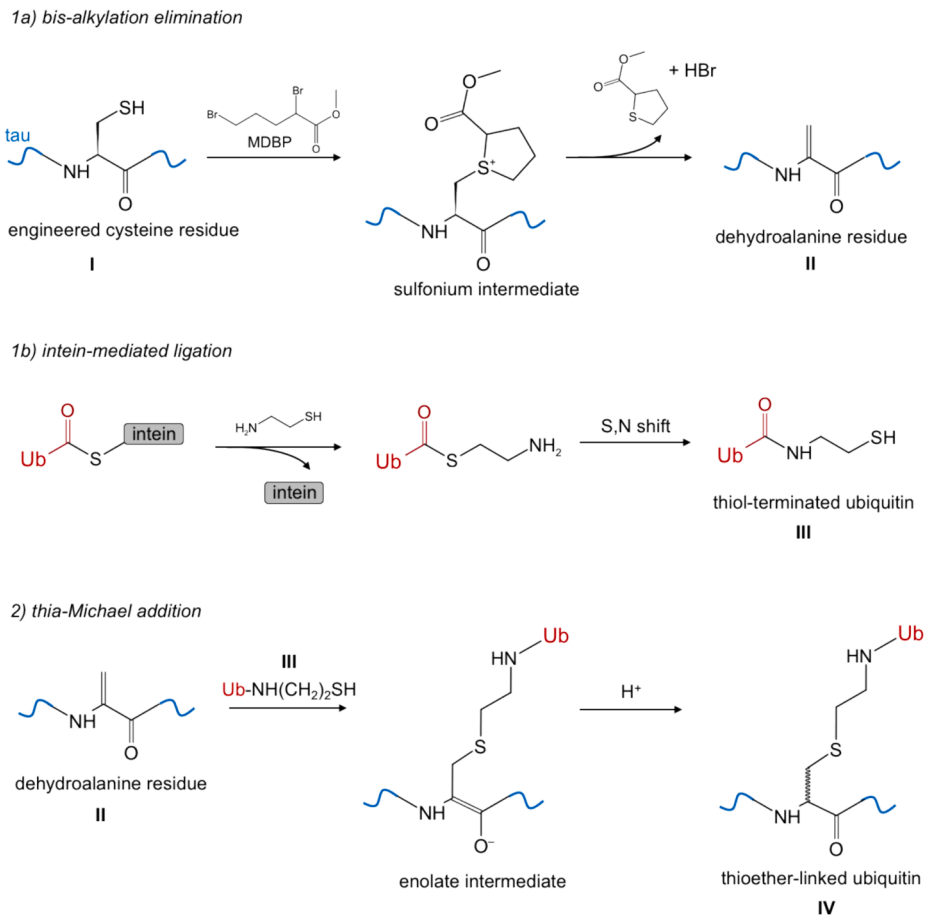

Scheme 1. Synthesis of ubiquitinated tau4RD via Dha chemistry.

structure may form transiently and potentially influence the self-interaction propensity of the polypeptide [45]. To gain insight into the conformational perturbations induced by Ub on the substrate tau4RD, the secondary structure of tau4RD(353)-S-Ub was examined by far-UV circular dichroism (CD). The spectrum of tau4RD$^{\Delta C}$(353Cys) displays a deep negative ellipticity minimum at ~ 198 nm and no major bands at wavelengths longer than 205 nm (Fig. 3A, black), in agreement with its disordered state. The spectrum of Ub reflects the presence of both β-sheet and α-helical elements of secondary structure (Fig. 3A, red). The spectral profile for the ubiquitinated proteoform (Fig. 3A, green) displays a negative dichroic signal at 202 nm and overall stronger negative ellipticity than unmodified tau4RD. Since the spectrum of tau4RD(353)-S-Ub coincides with the sum of the spectra of unconjugated protein moieties, within experimental error (Fig. 3A, dashed green line), it can be concluded that the overall fold of Ub and the disordered character of tau4RD were retained and no major secondary structure motifs were induced by the modification.

Complementary biophysical techniques are needed for a more in-depth characterization of the structure and dynamics of the conjugate. Nuclear magnetic resonance (NMR) spectroscopy is unique for its ability to provide atomic-level structural information on both folded proteins and highly dynamic polypeptides. Moreover, segmental labelling with ^{15}N- and/or ^{13}C isotopes enables the separate examination of distinct protein moieties or domains [46]. The chemical mutation strategy we have designed in this study proves ideal for NMR sample preparation. Here, we produced ^{15}N-enriched wild-type Ub-intein fusion protein to obtain the thiol-terminated [^{15}N]Ub derivative (Scheme 1, 1b). The latter was conjugated to the substrate with a one-step reaction to obtain selectively labelled tau4RD(353)-S-[^{15}N]Ub. We then recorded a ^{1}H-^{15}N HSQC spectrum of tau4RD(353)-S-[^{15}N]Ub and compared it with the unconjugated [^{15}N]Ub moiety (Fig. 3B). The ^{1}H-^{15}N HSQC signals of amide atom pairs are influenced by the local chemical environment and are exquisitely sensitive to variations in the protein structure or interactions. The superimposition of the spectra (Fig. 3B) shows that most of the signals of Ub were unaffected by the conjugation to tau4RD, confirming that Ub retained its native fold. However, the peaks of the C-terminal residues L69-L73 experienced chemical shift perturbations, and the amide peak of residue R74 disappeared, likely reflecting local conformational/dynamic changes of the flexible C-terminus upon linkage to tau.

The covalent conjugation of two protein moieties is expected to affect the global dynamic behavior of each component. Here, we examined global changes in the rotational diffusion of Ub via nuclear spin relaxation measurements [47]. Specifically, we determined the ^{15}N longitudinal relaxation time (T_1) of [^{15}N]Ub, both when conjugated to tau4RD and in the unconjugated form (Fig. S2). T_1 values were 575 ± 21 ms and 497 ± 26 ms (mean ± SD) for the conjugated and unconjugated Ub, respectively. T_1 is an indicator of the overall tumbling rate of the observed molecule, directly related to its shape and size; the difference in the observed values is consistent with the covalent addition of the tau4RD moiety.

2.3. Fibrils formation

To compare the aggregation kinetics of tau4RD(353)-S-Ub with that of the unconjugated protein, the in vitro fibrillization of tau4RD was followed by monitoring the time-dependent fluorescence signal of Thioflavin-T (ThT), a benzothiazole dye responsive to the cross-β structures characteristic of amyloid-like fibrils [48]. Most tau proteoforms and constructs, including tau4RD, are stable in solution as

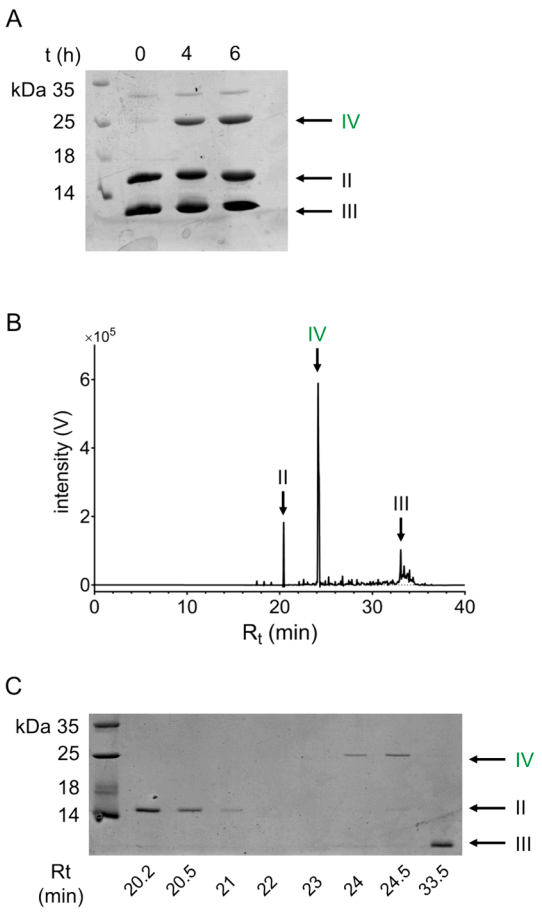

Fig. 1. (A) SDS-PAGE showing the time course of the reaction to obtain the ligated product **IV**. The bands of the reagents **II** and **III** are also visible. (B, C) HPLC chromatogram and SDS-PAGE analysis of the purification of the ligated product **IV**. The reagents and the product are indicated as in Scheme 1. Uncropped gels are shown in Fig. S7.

monomers, therefore aggregation inducers like heparin or fatty acids are generally used to probe the aggregation mechanism [49,50]. The kinetic profile of the two samples, in the presence of heparin, was sigmoidal-shaped and consistent with a macroscopic nucleation-growth mechanism (Fig. 4A). In the used conditions, both the nucleation and growth processes were rapid for unmodified tau4RD$^{\Delta C}$ (midpoint transition time constant, $t_{0.5} = 3.0 \pm 0.2$ h; elongation time constant, $\tau = 0.4 \pm 0.2$ h, Table S1). By contrast, a decreased aggregation rate was observed for tau4RD(353)-S-Ub ($t_{0.5} = 8.9 \pm 0.2$ h; $\tau = 0.7 \pm 0.2$ h), indicating that ubiquitination in position 353 disfavored protein self-assembly. As a control, we performed the aggregation assay on tau4RD(353)-S-Ub in the absence of inducer; as no increase in the fluorescence signal was observed, we exclude that the sole ubiquitin modification could promote tau aggregation (Fig. 4A). These results are in agreement with our previous finding obtained on a ubiquitinated tau4RD$^{\Delta C}$ produced exploiting disulfide-coupling chemistry (tau4RD(353)-S—S—Ub) [30,33]. It is plausible that the conjugation of Ub to residue 353 causes steric hindrance in a protein stretch that forms the ordered core of filaments, resulting in a reduced rate of self-assembly. Aggregation kinetics experiments performed at lower protein concentration (5 μM) indicated a slower aggregation rate, in agreement with previous studies [51,52], more evident when ubiquitin was bound to tau4RD (Fig. S3, Table S1).

The analysis of the aggregates by transmission electron microscopy (TEM) (Fig. 4B) confirmed that both samples, unconjugated and conjugated tau4RD, formed long mature fibrils, however with different morphology (Fig. S4). The incorporation of ubiquitinated tau proteoforms in filamentous aggregates is of utmost relevance since it has been proposed that ubiquitination, in combination with other PTMs, may affect the ultrastructural organization of pathological tau aggregates [5].

2.4. Stability assays under biological conditions

The question of whether tau ubiquitination regulates its aggregation or spreading during AD and other tauopathies is still open. Various *in vitro* studies show that site-specific ubiquitination of tau influences fibril formation [17,33,34]. However, further investigations using *in cell* and *in vivo* models are needed to shed light on possible mechanisms linking a

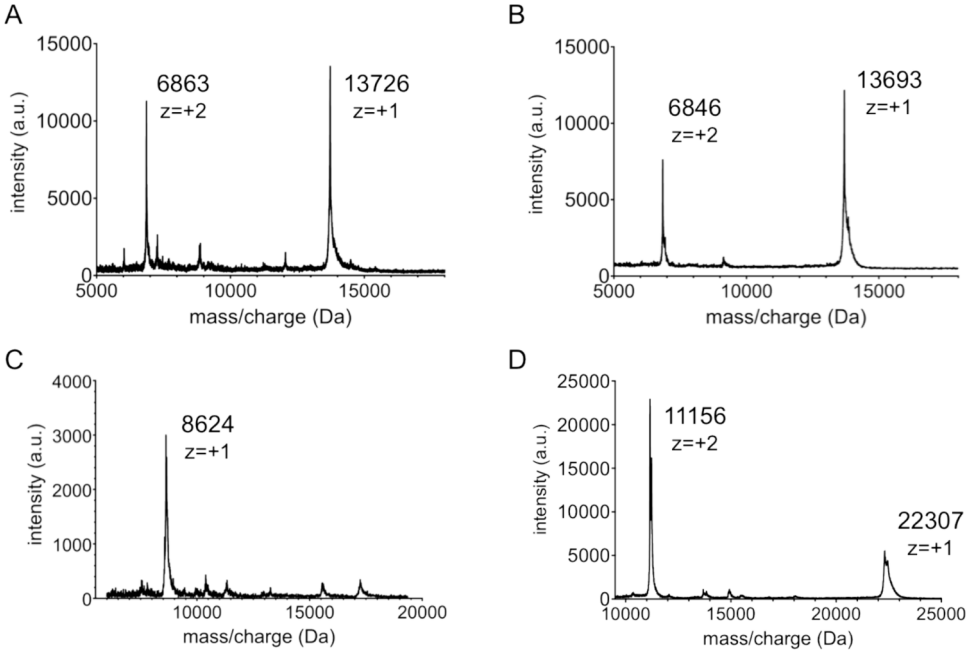

Fig. 2. Maldi-TOF mass analysis of (A) tau4RD$^{\Delta C}$(353Cys) **I** (calculated mass 13725 Da), (B) tau4RD$^{\Delta C}$(353Dha) **II** (calculated mass 13691 Da), (C) thiol-terminated ubiquitin **III** (calculated mass 8624 Da), (D) ligated product tau4RD(353)-S-Ub **IV** (calculated mass 22315 Da).

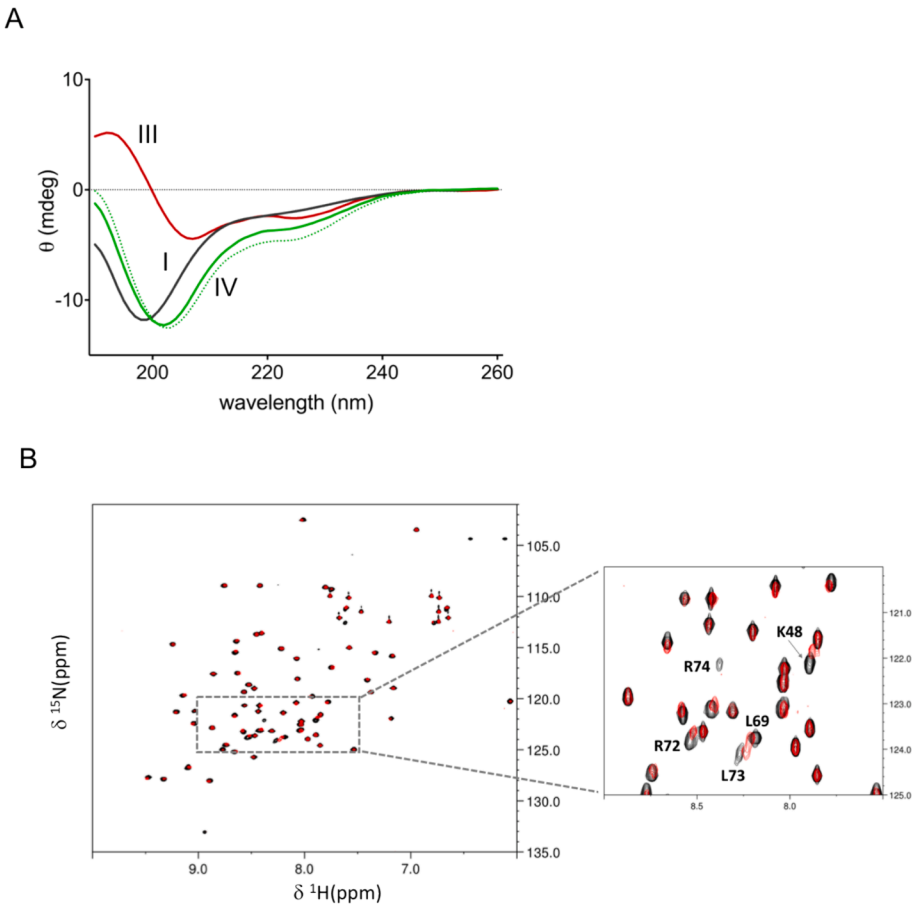

Fig. 3. (A) Far-UV CD spectra recorded on 6 μM tau4RD$^{\Delta C}$(353Cys) **I**, thiol-terminated ubiquitin **III**, and ligated product tau4RD(353)-S-Ub **IV**. The sum of the spectra of **I** and **III** is represented with a green dashed line. Spectra were recorded at 25 °C. Samples were prepared in milliQ water. (B) Overlay of the ^{1}H-^{15}N HSQC NMR spectra of ^{15}N-ubiquitin wild type (black), and tau4RD(353)-S-[^{15}N]Ub displaying signals solely of the ^{15}N-enriched conjugated ubiquitin moiety (red), in the right panel a zoom of the central region between 9 and 7.5 ppm and 125 and 120 ppm is shown. Spectra were recorded using a 600 MHz NMR spectrometer at 25 °C. Proteins were at concentration of 100 μM in 20 mM sodium phosphate buffer at pH 6.8, added with 7 % D_2O.

complex PTM, ubiquitination, to tau aggregation and pathology.

In this context, understanding the effects of biological media on the newly formed chemical bond stability of the synthesized conjugate, tau4RD(353)-S-Ub, is paramount. When performing *in cell* studies, the protein sample interacts with the components of the culture medium prior to any cellular contact. Here, we evaluated the chemical stability over time of the tau4RD(353)-S-Ub conjugate, after dissolving the protein in a multi-component buffer (PBS) or three commonly used cell culture media (DMEM, DMEM + FBS, EBBS), performing an immunoblot analysis with an anti-tau antibody (Fig. 5). In all blots, under different conditions, a single band is visible with constant intensity over time, indicating that the constituents of the biological media (macromolecules, small molecules, ionic salts, etc) did not affect the stability of the conjugate.

Next, we analyzed the behavior of tau4RD(353)-S-Ub in more complex biological systems. *E. coli* cell extracts were obtained from cultures of the BL21(DE3) strain grown in LB-rich medium and then lysed via sonication steps. A variety of components such as ions, metabolites, lipids, and large macromolecules characterizes *E. coli* cell extracts, [53,54] providing a diverse pool of biomolecules to test the chemical stability of the synthesized product tau4RD(353)-S-Ub. The immunoblot analysis showed that no additional bands appeared upon incubation of the conjugate up to 48 h, demonstrating the chemical stability of the thioether bond in this biological medium (Fig. 6A). We further evaluated the behavior of the protein in human serum, which is characterized by a different chemical and biological composition than the bacterial extract [55]. Similarly to what observed in the bacterial extract, the band of the sample did not decrease in intensity over time, again supporting the chemical stability of the conjugate for up to 48 h of incubation (Fig. 6B). For comparison, we performed the same set of experiments using a conjugate produced exploiting disulfide-coupling chemistry, referred to as tau4RD(353)-S—S—Ub [17,33] (Fig. S5). The band of the latter conjugate was no more visible in the blots acquired after 24 or 48 h (Fig. 6), proving lower chemical stability over time of tau4RD(353)-S—S—Ub with respect to tau4RD(353)-S-Ub, both in *E. coli* extracts and human serum.

Experiments for biomedical research often involve the employment of mammalian cell line cultures. In view of using tau4RD(353)-S-Ub for this kind of experiments, we tested the chemical stability of the bioconjugate under physiological conditions using two culture media containing intact and lysed Hek293T cells, respectively (Fig. 7). The composition of the two media is different. The first mainly consists of nutrients, macromolecules, and metabolites secreted and accumulated during cell growth [56], while the second, more complex, consists of a variety of small molecules, portions of cellular membranes, proteins, and components of the machinery necessary for cell growth and survival [57]. From immunoblot analysis, we observed that the band of the conjugate tau4RD(353)-S-Ub, at a concentration of 7 μM, was present up to 8 h of incubation in the two media and disappeared after 24 h, in both conditions (Fig. 7). By comparison, the band of the sample tau4RD(353)-S—S—Ub was slightly visible up to 8 and 4 h of incubation in media of intact and lysed cells, respectively, and increasing intensity of the band of tau4RD was observed over time (Fig. 7), suggesting a breakdown of the disulfide bond. These data clearly indicate improved stability of the

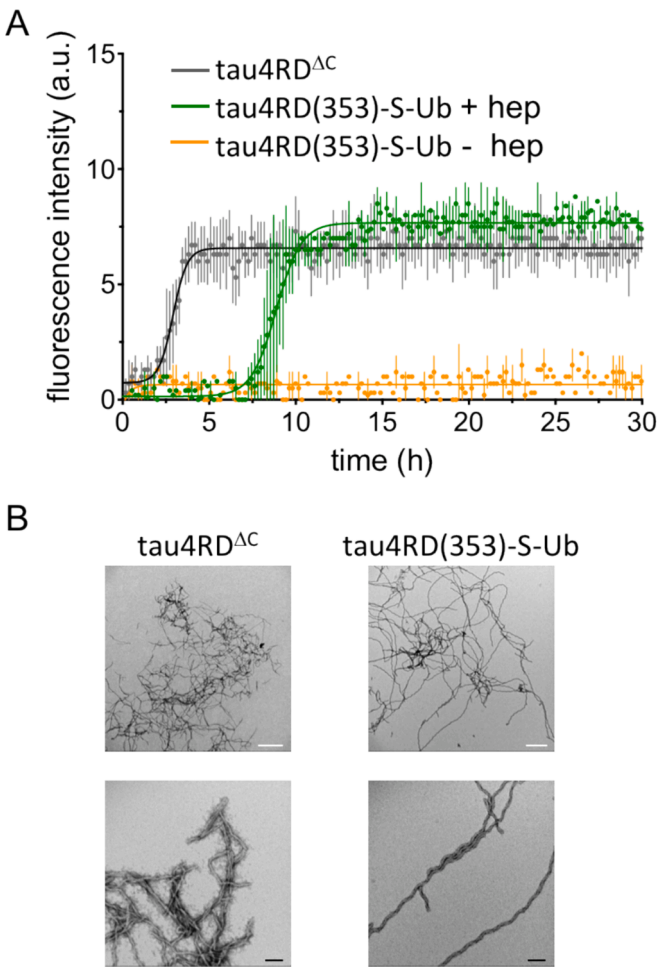

Fig. 4. (A) ThT fluorescence assay on tau4RD$^{\Delta C}$ and tau4RD(353)-S-Ub incubated with heparin (1:1 ratio); the assay is performed also on tau4RD(353)-S-Ub incubated without heparin, as control. Measurements were performed in triplicate on 10 μM protein samples; data represent the mean ± SD. Solid lines correspond to the best-fit curves determined using the empirical sigmoid function indicated in the Materials and Methods section. (B) Representative TEM images of aggregates of tau4RD$^{\Delta C}$ (left panels), and tau4RD(353)-S-Ub (right panels), formed after 48 h incubation of proteins in aggregating conditions. Scale bars: 500 nm (white) and 100 nm (black).

newly synthesized conjugate tau4RD(353)-S-Ub in cell culture media, compatible with the incubation times typical of *in cell* experiments.

2.5. Internalization by astrocytes

Tau protein is prevalently found in neurons, however its deposits are frequently found in astrocytes in a variety of tauopathies [58]. The astrocytes do not express tau, the mechanisms driving the appearance of tau aggregates and their involvement in disease progression are still largely unknown, and recent studies established that astrocytes play a central role in mediating tau pathology [59]. Therefore, we decided to investigate if the synthesized conjugate, tau4RD(353)-S-Ub could be successfully internalized by astrocytes in primary cultures obtained from the cerebral cortices of newborn (P0-*P2*) triple transgenic (3xTg-AD) mice. The latter is a widely used model of Alzheimer's disease that overexpresses mutated human proteins associated with early-onset disorder (APPswe, Psen-1, and tau) and reproduces both Aβ and tau pathology [60,61].

The primary astrocyte cultures obtained from 3xTg-AD mice were treated with 5 μM of tau4RD(353)-S-Ub labeled with fluorescein isothiocyanate or with culture medium as a control, for either 4 or 24 h. To verify the internalization of the conjugate, after fixation and staining with the nuclear marker Dapi and the astrocyte marker GFAP, the confocal microscopy images were analyzed through the creation of a colocalization channel of GFAP and tau4RD(353)-S-Ub (Fig. 8A-B). We also treated astrocytes with monomeric tau4RD and verified that it was successfully internalized in agreement with previous studies (Fig. S6) [62].

Most astrocytes treated with tau4RD(353)-S-Ub showed colocalization of GFAP and the conjugate (Fig. 8). Quantitative analysis (Fig. 8C) indicated that the conjugate was efficiently internalized already after 4 h of incubation, and no significative differences were observed with longer incubation time. Our experiments revealed that the astrocytes of an animal model of AD successfully internalized the synthesized conjugate tau4RD(353)-S-Ub at both treatment times.

3. Conclusions

In summary, we developed a novel chemical mutagenesis strategy that enables the synthesis of site-specific ubiquitin protein conjugates via a Dha precursor. We successfully applied the protocol to prepare ubiquitin-tau4RD (a shorter construct of tauFL) with good yield and high purity. The synthetic strategy can be easily adapted for synthesizing any ubiquitinated tau proteoform, including tauFL protein. The advantage of this method is the possibility of obtaining samples of ubiquitinated tau4RD which can be employed in a variety of experiments, both for structural and *in cell* studies. We demonstrated that the structural characteristics of the two moieties, ubiquitin and tau4RD, remained unchanged upon conjugation, and showed that tau4RD maintained its ability to form fibrils in the presence of ubiquitin bound at position 353, although with different kinetics. Our method also allowed the NMR-based inspection of the Ub modifier, which is of great value to elucidate if the interactions of ubiquitinated tau could have a role in pathology, as the noncovalent interactions of Ub with cognate biomolecules orchestrate numerous Ub-dependent cellular signaling pathways. Moreover, we tested the chemical stability of the conjugate in a variety of biological media and showed that tau4RD(353)-S-Ub remained stable for several hours and, in some biological environments, up to 48 h. As a proof of concept, we further demonstrated

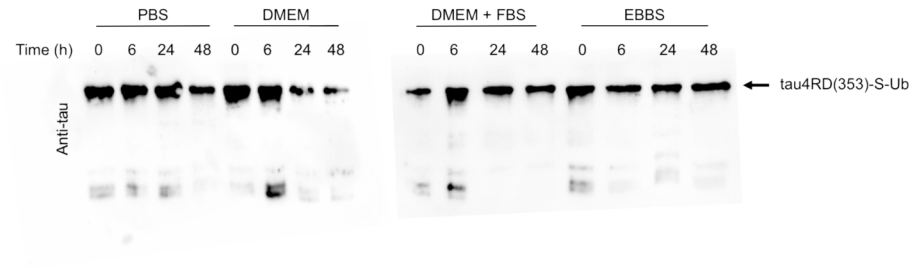

Fig. 5. Immunoblot analysis of long-term stability of the conjugated product tau4RD(353)-S-Ub in different biological buffers and media, performed with anti-tau antibody. Uncropped blots are shown in Fig. S7.

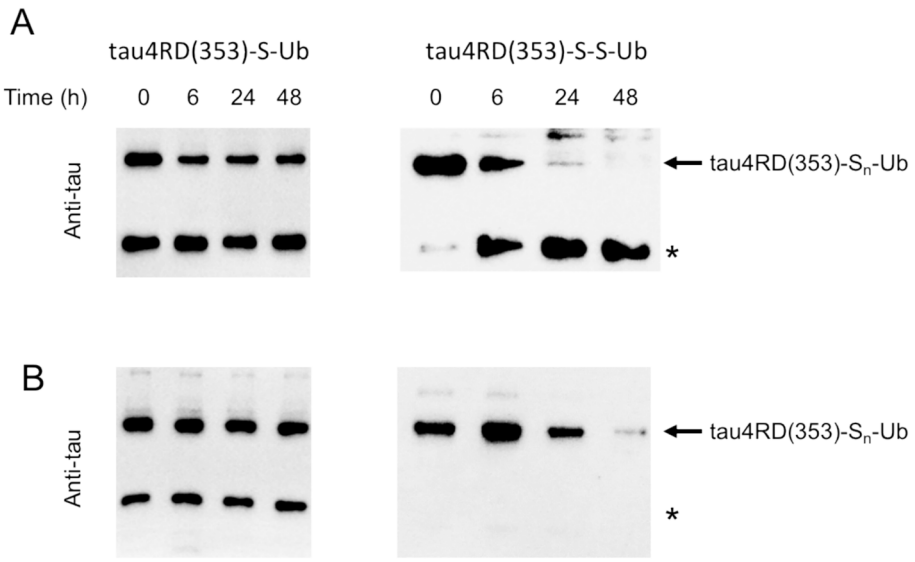

Fig. 6. Immunoblot analysis of long-term stability of the conjugated product tau4RD(353)-S-Ub in comparison with tau4RD(353)-S—S—Ub in (A) *E. coli* extracts, and (B) human serum, performed with anti-tau antibody. The asterisks indicate bands with MW compatible with tau4RD constructs. Uncropped blots are shown in Fig. S7.

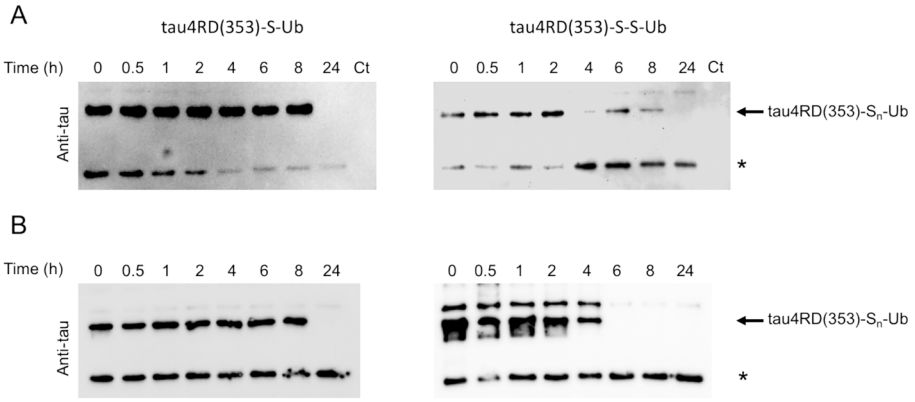

Fig. 7. Immunoblot analysis of long-term stability of the conjugated product tau4RD(353)-S-Ub in comparison with tau4RD(353)-S—S—Ub in a culture media of Hek293T (A) intact or (B) lysed cells, performed with anti-tau antibody. The negative controls (Ct) were obtained collecting samples of the culture medium of Hek293T intact cells before proteins addition. The asterisks indicate bands with MW compatible with tau4RD constructs. Uncropped blots are shown in Fig. S7.

efficient internalization of the conjugate into mouse cortical astrocytes.

Altogether, the described approach offers a precise chemical tool to achieve stable tau4RD conjugation with ubiquitin, paving the way for future *in vitro*, *in cell*, and *in vivo* experiments that can contribute to shed light onto the physiological and pathological mechanisms involving tau ubiquitination, which has remained one of the most elusive PTMs of tau.

4. Materials and methods

4.1. Chemical reagents, antibodies and biological media

Methyl 2,5-dibromopentanoate (MDBP) was purchased from BLDpharm (Germany). Isopropyl-β-D-1-tiogalattopiranoside (IPTG), Heparin (cat # H3393, average MW 18 kDa), Thioflavin-T (ThT), HPLC-grade acetonitrile, dithiothreitol (DTT), 5,5 dithio-bis-(2-nitrobenzoic acid) (DTNB) and Trifluoroacetic acid (TFA) were purchased from Sigma-Aldrich (St Louis, MO, USA).

Antibodies: anti-GFAP (Rat, cat # 13–0300) and goat anti-rat Alexa Fluor 647 (cat # A21247, 1:1000) were purchased from Thermo Fisher Scientific (Waltham, MA, USA,); DAPI (4′,6-diamidino-2-phenylindole, cat #D9542, 1:5000) was purchased from Merck Millipore.

Phosphate Buffer Solution w/o calcium and magnesium (PBS), Dulbecco's Modified Eagle medium (DMEM) high glucose w/ stable glutamine w/ sodium pyruvate, Fetal Bovine Serum (FBS) were purchase from Biowest (Nuaillé FR), Earle's Balanced Salt Solution (EBSS) from Thermo Fisher (Waltham, MA, USA).

In all preparations, high-purity deionized water from a Millipore system was used.

4.2. Recombinant proteins expression and purification

Tau4RD.

The mutants C291A/C322A (hereafter tau4RD$^{\Delta C}$) and C291A/C322A/K353C (hereafter, tau4RD$^{\Delta C}$(353Cys)) were obtained by site-directed mutagenesis starting from the plasmid of tau4RD (residues Q244-E372 of human full-length tau, plus initial Met). All the constructs were expressed and purified as described previously [17].

Briefly, the proteins were expressed in BL21(DE3) cells grown in LB medium at 37 °C for 5 h, after induction obtained by addition of 0.5 mM IPTG. Protein purification was achieved by thermal treatment of the soluble bacterial extract (80–100 °C) and SP-ion exchange chromatography. Purified tau4RD$^{\Delta C}$ constructs were dialyzed in water.

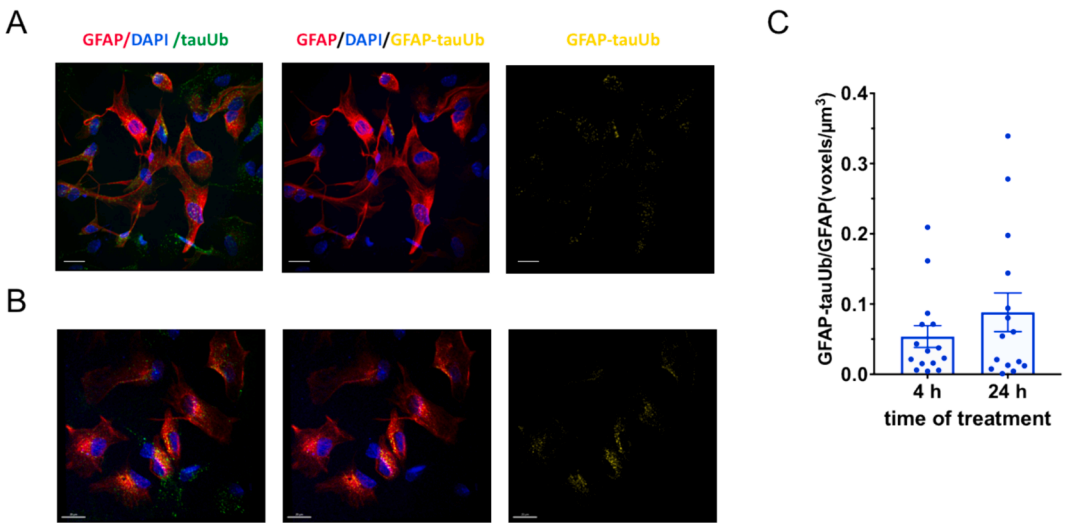

Fig. 8. Immunofluorescence analysis of internalization of tau4RD(353)-S-Ub (indicated as tauUb) by astrocytes. Representative images of primary mouse cortical astrocytes maintained in culture for 7 DIV, treated with 5 μM of tau4RD(353)-S-Ub (green) for (A) 4 and (B) 24 h and immunolabelled with nuclear marker DAPI (blue), and astrocytic marker GFAP (red) (left and middle panels). In the middle and right panels the channel of colocalization of GFAP and tau4RD(353)-S-Ub is shown (yellow). Scale bar: 20 μm. The fluorescent conjugate tau4RD(353)-S-Ub was obtained with fluorescein isothiocyanate (FITC). (C) Quantitative analysis of GFAP-tau4RD(353)-S-Ub positive on the total GFAP positive expressed as the number of voxels on the total cells volume (mean ± SEM; N = 15). The analyzed images were obtained from 3 experiments for each group.

Ubiquitin wild type.

The Ub was produced in Rosetta cells grown in LB medium at 37 °C for 5 h and purified as described [63].

Ub-GyrA-Int-His.

The Ub-intein-His protein was produced in BL21(DE3) cells at 37 °C in auto-inducing medium and purified as previously described by immobilized nickel affinity chromatography (IMAC) according to standard protocols [34].

Ub-SH.

Ub-SH was obtained by incubating the clean fusion Ub-intein-His protein in a buffer containing Tris-HCl 20 mM at pH 7.5, EDTA 1 mM, cysteamine 40 mM, and Tris(2-carboxyethyl) phosphine (TCEP) 3 mM for 48 h at room temperature. Ub-SH was purified by superdex-75 gel filtration column with 20 mM Tris-HCl pH 7.5 and 150 mM NaCl buffer. Purified Ub-SH was dialyzed in water. The protein was verified by MALDI-TOF/TOF mass spectrometry (Fig. 2C).

4.3. Dha formation

The tau4RD$^{\Delta C}$(353Dha) was obtained according to previous protocols [38]. Briefly, the tau mutant tau4RD$^{\Delta C}$(353Cys) was buffer exchanged into 20 mM sodium phosphate buffer (pH 8) via G-25 M Sephadex PD-10 desalting column (GE Healthcare). Then 500 μL aliquots of 800 μM protein were reacted with 50 mol equivalent of methyl MDBP for 6 h at 37 °C and with shaking at 500 rpm (IKA matrix orbital, IKA-Werke GmbH & Co. KG, Staufen, Germany). Excess of MDBP was removed using a G-25 M Sephadex PD-10 desalting column. The conversion of the cysteine to Dha was verified via MALDI-TOF/TOF mass spectrometry (Fig. 2B).

4.4. Chemical mutagenesis

To synthesize the ubiquitinated tau4RD, tau4RD$^{\Delta C}$(353Dha) and thiol-terminated ubiquitin Ub-SH were reacted in a molar ratio 1:3, in the presence of 3 eq. of DTT. The mixture was left to react for 6 h at 37 °C under shaking at 700 rpm (IKA matrix orbital, IKA-Werke GmbH & Co. KG, Staufen, Germany). Excess of DTT was removed via G-25 M Sephadex PD-10 desalting column. The product of the reaction was then purified via HPLC chromatography.

4.5. Disulfide-directed monoubiquitination reaction

To synthesize the sample tau4RD(353)-S—S—Ub we exploited an already described protocol based on a disulfide-directed reaction [17,34]. Briefly, the thiol-terminated ubiquitin Ub-SH was incubated with excess of DTNB in 100 mM Hepes pH 7.0 overnight at 10 °C. After the activation reaction, the TNB excess was removed using a PD10 desalting column, and the activated ubiquitin was incubated for 1 h at room temperature with tau4RD$^{\Delta C}$(353Cys) in a 1:4 tau:ubiquitin molar ratio. The semisynthetic ubiquitination reaction was performed in 100 mM Hepes buffer, pH 7.0, and 3 M urea. To avoid the formation of dimers, tau4RD$^{\Delta C}$(353Cys) was previously treated with 20 mM DTT, which was removed using a PD10 desalting column before the conjugation reaction. The tau4RD(353)-S—S—Ub conjugate was then purified through ion exchange chromatography. The purity was determined by SDS-PAGE, and the mass was verified by mass spectrometry (MALDI-TOF) (Fig. S5). The total reaction yield was about 30 %.

4.6. HPLC purification

The conjugate tau4RD(353)-S-Ub was purified by HPLC chromatography. Samples of 1 mL of the reaction pool were injected in a reverse-phase HPLC column (Jupiter C4, 5 μm, 300 Å, size 250 cm × 4.6 mm). The unreacted reagents and the product were eluted at room temperature using a linear gradient of H_2O/acetonitrile (20–50 %) with 0.1 % trifluoracetic acid (flow rate of 5 mL/min). The HPLC elution profile was monitored at 280 nm. The fractions were collected and analyzed with SDS-PAGE. Tau4RD(353)-S-Ub was eluted with the 37 % of acetonitrile, which was then removed by several washes in water with 3KDa cut-off filter (Merck, Darmstadt, Germania).

4.7. Far-UV circular dichroism spectroscopy

Circular Dichroism (CD) measurements were carried out on a Jasco J-1500 spectropolarimeter equipped with a Peltier type temperature-controlled cell holder (Jasco, Easton, MD, USA). Far-UV spectra (190–260 nm) were recorded in 0.1 cm cuvettes, at 25 °C, with a scan rate of 50 nm min^{-1}, a bandwidth of 1 nm, and an integration time of 2 s. Five spectra accumulations were averaged for each sample and the

spectrum of the buffer was considered as a blank and subtracted. The protein concentration was 6 μM in milliQ water. Data plots were generated with GraphPad Prism 9 (GraphPad Software Inc., La Jolla, CA, USA).

4.8. NMR spectroscopy

^{15}N-labeled ubiquitin samples for NMR experiments were obtained growing the cells in M9 minimal medium supplemented with 1 g/L $^{15}NH_4Cl$ as the sole source of nitrogen. All samples were prepared in 20 mM potassium phosphate buffer at pH 6.8, containing 7 % D_2O. Proteins concentration was 100 μM. NMR spectra were recorded at 25 °C on a 600 MHz Bruker Avance III Ultrashield plus spectrometer equipped with a triple resonance TCI cryogenic probe. Two-dimensional ^{1}H-^{15}N HSQC spectra were acquired with a data matrix consisting of 2048 (F2, ^{1}H) × 256 (F1, ^{15}N) complex points, 8 scans, 1.2 s recycle delay, and spectral widths of 7143 (F2, ^{1}H) and 2190 (F1, ^{15}N) Hz. NMR data were processed and analyzed with Topspin 3.6.2 (Bruker, Karlsruhe).

4.9. Thioflavin-T (ThT) aggregation assay

Prior to running aggregation assays, solutions of tau4RD were filtered through a 100 kDa cut-off filter (Sartorius Stedim Biotech GmbH, Göttingen, Germany) to remove pre-existing large oligomers and fibrils. The aggregation was induced by incubating the protein with heparin, both at 10 μM concentration, in 20 mM phosphate buffer, 50 mM NaCl and 2 mM DTT.

The kinetics of aggregation was monitored by measuring the fluorescence of ThT (10 μM) added to each sample in a 96-well dark plate (100 μL final volume in each well). Fluorescence measurements were performed using a TECAN Infinite M200 Pro microplate reader (Tecan Group AG, Männedorf, Switzerland) at 30 °C for ca. 72 h with cycles of 30 s of shaking (250 rpm, orbital) and 10 min of rest throughout the incubation. The fluorescence intensity was measured every 11 min (excitation, 450 nm; emission, 480 nm; bottom read).

Error bars of fluorescence data correspond to standard deviations of three independent experiments.

The following sigmoidal function was employed to fit each individual experimental data set to analyze the aggregation kinetics:

$$y = y_i + \frac{y_f}{1 + e^{-[(t-t_{0.5})/\tau]}}$$

where y is the fluorescence intensity as a function of time t, y_i and y_f are the intercepts of the initial and final baselines with the y-axis, $t_{0.5}$ is the time needed to reach halfway through the elongation phase, and τ is the elongation time constant. The lag time is defined as $t_{lag} = t_{0.5} - 2\tau$. The values reported in the text correspond to the mean ± SD of the individual values computed separately on each curve.

4.10. Transmission electron microscopy (TEM)

For TEM measurements, samples were prepared as described for the ThT assay in the final volume of 100 μL and incubated at 30 °C for 48 h in static conditions. Subsequently, 30 μL of aggregated samples (5 μM) in milliQ water were adsorbed onto 400 mesh holey film grids; after staining with 2 % uranyl acetate (for 2 min), the sample was observed with a Tecnai G^2 (FEI) transmission electron microscope operating at 100 kV. Images were captured with a Veleta (Olympus Soft Imaging System, Münster, Germany) digital camera using FEI TIA acquisition software (Version 4.0).

4.11. Mass spectrometry

Mass spectra were acquired on a Bruker Ultraflextreme MALDI-TOF/TOF instrument (Bruker Daltonics, Billerica, MA, USA). Samples were acidified with TA30 solution (30 % Acetonitrile, 0.1 % trifluoroacetic acid in water). The resulting solutions were mixed 1:1 (v/v) with the matrix HCCA (α-cyano-4-hydroxycinnamic acid) and 1 μL of the sample/matrix solution was spotted in triplicate onto a Ground steel MALDI target plate (Bruker Daltonics) and dried at room temperature.

4.12. Samples preparation for Western blots analysis

Cell culture media and reagents.

Dulbecco's modified Eagle's medium (DMEM), Earle's balanced salt solution (EBSS), fetal bovine serum (FBS) and phosphate-buffered saline (PBS) were ready-to-use solutions. The conjugate tau4RD(353)-S-Ub was incubated with 100 μL of each medium at a final concentration of 7 μM. Samples were collected over time, diluted in gel loading buffer and stored at −80 °C.

E. coli extracts.

Cell extracts were prepared from *E. coli* BL21(DE3) cells cultures. 100 μL of BL21(DE3) cells were inoculated into 50 mL of LB medium. Cell growth was monitored by OD_{600} absorbance and when it reached 0.6 the cells were harvested by centrifugation at 10,000 g for 15 min. The pellet was resuspended in 1 mL of lysis buffer containing DNAse, 1 mg lysozyme, protease inhibitors, 5 mM $MgCl_2$ and 1 mM EDTA. The solution was sonicated five times for 1 min alternating with periods of rest on ice. The lysate was then centrifuged at 10,000 g for 20 min, the pellet was discarded, and the supernatant was lyophilized and stored at 4 °C.

For stability assays, the lyophilized extract was resuspended in 2 mL of PBS buffer and 100 μL were then added with 0.02 % NaN_3, protease inhibitors and 7 μM of tau4RD(353)-S-Ub or tau4RD(353)-S—S—Ub. The samples containing tau4RD(353)-S-Ub were added with 2 mM of DTT. All the samples were incubated at 25 °C in static conditions. Samples were taken over time, diluted in gel loading buffer and stored at −80 °C.

Human serum.

Human serum was extracted from the blood of a donor. Blood samples were collected in serum separator tubes without anticoagulant; they were allowed to clot for at least 30 min, then centrifuged at 1100 g for 10 min to separate the clot. Human blood serum was aliquoted and frozen at − 80 °C immediately after centrifugation.

For stability assays, 100 μL of the aliquot of the human serum were diluted in 900 μL of PBS buffer. Samples of 100 μL of human serum were supplemented with 0.02 % NaN_3, protease inhibitors and 7 μM of tau4RD(353)-S-Ub or tau4RD(353)-S—S—Ub. The samples containing tau4RD(353)-S-Ub were added with 2 mM of DTT. All the samples were incubated at 25 °C in static conditions. Samples were taken over time, diluted in gel loading buffer and stored at −80 °C.

Hek-293 T cells.

Hek-293 T cells were cultured in a humidified atmosphere of 5 % CO_2 in DMEM High Glucose with 10 % FBS and 1 % penicillin–streptomycin. The cells were plated at a density of 2.2×10^6 cells for a 10 cm dish and then harvested with trypsin. Next, for stability assays, 1 mL of living cells (1.3×10^6 cells) was centrifuged for 1 min at 3000 g and resuspended in 500 μL of PBS, and lysed with triton buffer (1 % Triton X-100 in 50 mM Tris, 150 mM NaCl, pH 7.6), containing protease inhibitors and 0.02 % NaN_3. The stability assays were performed incubating 7 μM of tau4RD(353)-S-Ub or tau4RD(353)-S—S—Ub in each medium for 48 h at 25 °C in static conditions. Samples were collected over time, diluted in gel loading buffer and stored at −80 °C.

Samples analysis by Western blot.

All samples were separated by sodium dodecyl sulphate–polyacrylamide gel electrophoresis (SDS-PAGE) and probed with the "Purified anti-Tau, 359–373" antibody (Biolegend). Immuno-reactive proteins were detected using an enhanced chemiluminescence reagent (Ge Healthcare) according to the manufacturer's instructions.

4.13. Fluorescent labeling of tau4RD$^{\Delta C}$ and tau4RD(353)-S-Ub

Fluorescein isothiocyanate (FITC) was conjugated to tau4RD$^{\Delta C}$ or tau4RD(353)-S-Ub by adding 20 μL of FITC in DMSO (2 mg/mL) to 200 μL of proteins (2 mg/mL), in 0.1 M bicarbonate buffer solution, pH 9. The mixture was left to react for 2 h at room temperature under stirring. The unconjugated dye was removed via G-25 M Sephadex PD-10 desalting column and the (FITC)tau4RD$^{\Delta C}$ or (FITC)tau4RD(353)-S-Ub eluted in milliQ water. The (FITC)tau4RD$^{\Delta C}$ and (FITC)tau4RD(353)-S-Ub samples were then lyophilized and resuspended in 50 μL of sterile water. Labeling efficiency was estimated based on relative concentrations of the protein and the dye (the latter determined by absorbance at 494 nm).

4.14. Animals

A colony of triple-transgenic AD mice (3xTg-AD) expressing three mutant human transgenes—PS1M146V, APPSwe, and tauP301L—was established at the University of Verona by purchasing transgenic mice from The Jackson Laboratory (Sacramento, CA, USA). Mice were housed at 3/cage at a constant room temperature of 21 ± 1 °C and maintained on a 12:12 h light/dark cycle with lights on at 7.30 a.m. with freely available food and water. All efforts to minimize animal suffering and number were made. The animal study protocol was approved by the Ethics Committee of the University of Verona and the Italian Ministry of Health.

4.15. Primary astrocytes cultures

Astrocytes were prepared from the cerebral cortices of P0-*P*2 mice as previously described[62] with some modifications. Cortices were dissected on 1X ice-cold DPBS (14200075, Thermo Fisher Scientific). After removal of meninges, cortices were enzymatically digested with DPBS solution containing 0.25 % (v/v) trypsin (15090046, Thermo Fisher Scientific), 1 mM sodium pyruvate, 0.1 % (w/v) glucose, 10 mM HEPES pH 7.3 for 20 min at 37 °C. Following 5 min of incubation with 0.1 mg/ml DNAse I (D4627, Sigma-Aldrich) at room temperature, the enzymatic reaction was stopped with a MEM (51200, Thermo Fisher Scientific) solution containing 10 % FBS (10270106, Thermo Fisher Scientific), 0.45 % (w/v) glucose, 1 mM sodium pyruvate, 2 mM L-Glutamine (25030081, Thermo Fisher Scientific), 100 U/mL penicillin, 100 μg/mL streptomycin (15140, Thermo Fisher Scientific). After trituration through a P1000 pipette, the cell suspension was passed through a 70 μm MACS SmartStrainer (Miltenyil Biotec). Then, cells were diluted in MEM containing 20 % FBS, 33 mM glucose, 2 mM L-Glutamine, 100 U/ml penicillin, 100 μg/ml streptomycin and seeded in a T75 cm^2 flask and were grown for two more weeks. Next, cells were trypsinized and seeded at a density of 120.000 cells/ml on poly-L lysine coated 12-mm coverslips of a 24-well plate and treated after 3 days. Cells were maintained in a standard, humidified 5 % CO_2 incubator until the day of the experiments. Astrocytes were exposed to either culture medium as negative control or (FITC)tau4RD(353)-S-Ub at a concentration of 5 μM for 4 or 24 h before being fixed.

4.16. Immunofluorescence

Primary cortical cells were fixed in 10 % (v/v) formalin solution (Titolchimica) for 15 min at room temperature, washed three times in PBS, blocked in PBS containing 10 % (v:v) normal goat serum (Thermo Fisher Scientific), and permeabilized with 0.3 % (v:v) TritonX-100 (Merck Millipore) in PBS for 40 min. Next, cells were incubated with rat anti-GFAP primary antibodies overnight at 4 °C, and after three PBS washing steps, with anti-secondary antibodies anti-rat Alexa Fluor 647 for 1 h at room temperature. Antibodies were diluted in PBS containing 5 % (v:v) normal goat serum. Nuclei were counterstained with DAPI 1:5000 and coverslips were mounted on slides using DAKO fluorescence mounting media (Agilent, Santa Clara, CA, USA). Images of different Z-planes were collected on a Leica tcs-sp5 confocal microscope. Images were processed with the software Imaris (Bitplane AG, Belfast, UK).

4.17. Image analysis

To verify and quantify the internalization of tau4RD$^{\Delta C}$ or tau4RD (353)-S-Ub by astrocytes the images were analyzed using the IMARIS® software 9.7. The analysis protocol starts with the application of a Gaussian filter (0.240 μm) and a threshold cut-off for the red channel to remove the unspecific signal that changes for each experiment. To verify the presence of (FITC)tau4RD$^{\Delta C}$ or (FITC)tau4RD(353)-S-Ub inside the astrocytes, we created two colocalization channels between the (FITC)tau green signal and the red of astrocytes. We manually selected the proper intensity range for all the signals, which are different for each experiment. The outcome of this colocalization is the creation of a new channel visualized as 3-dimensional pixels called voxels. To avoid results misinterpretation due to the different number of cells in the field, we normalized the number of voxels on the total cells' volume calculated through the proper IMARIS® function. This process required the manual selection of an area able to cover all cells without taking in consideration very low signals.

CRediT authorship contribution statement

Giovanna Viola: Validation, Methodology, Investigation, Formal analysis. **Daniele Trivellato:** Validation, Investigation. **Lorenzo Meulli:** Validation, Investigation, Formal analysis. **Roberto Tira:** Validation, Investigation. **Angela Lauriola:** Resources. **Francesca Munari:** Investigation. **Martina Montagnana:** Resources. **Mario Buffelli:** Writing – original draft, Validation, Investigation. **Michael Assfalg:** Writing – original draft, Visualization, Validation, Supervision. **Mariapina D'Onofrio:** Writing – review & editing, Writing – original draft, Visualization, Validation, Supervision, Methodology, Funding acquisition, Formal analysis.

Declaration of competing interest

The authors declare that they have no known competing financial interests or personal relationships that could have appeared to influence the work reported in this paper.

Acknowledgements

Centro Piattaforme Tecnologiche of the University of Verona is acknowledged for providing access to the microscopy, spectroscopy, and mass spectrometry facilities. The University of Padova is acknowledged for providing access to the Electron Microscope (DiBio Imaging Facility). The graphical abstract was created with BioRender.com.

This work was supported by a grant from the Alzheimer's Association (AARG-17-529221, M.D.). The work was also supported by the PNRR (National Recovery and Resilience Plan) PE00000006 "MNESYS —A Multiscale integrated approach to the study of the nervous system in health and disease", Mission 4, Component 2, Investment 1.3, funded by the European Union – NextGenerationEU, CUP B33C22001060002 to LM and RT (fellowships), MB and MA.

Appendix A. Supplementary data

Supplementary data to this article can be found online at https://doi.org/10.1016/j.bioorg.2024.107549.

References

[1] C.A. Ross M.A. Poirier Protein aggregation and neurodegenerative disease Nat Med 10 Suppl 2004 S10 S7.

[2] V.M. Lee, M. Goedert, J.Q. Trojanowski, Neurodegenerative tauopathies, Annu Rev Neurosci 24 (2001) 1121–1159.

[3] A.W.P. Fitzpatrick, B. Falcon, S. He, A.G. Murzin, G. Murshudov, H.J. Garringer, R. A. Crowther, B. Ghetti, M. Goedert, S.H.W. Scheres, Cryo-EM structures of tau filaments from Alzheimer's disease, Nature 547 (7662) (2017) 185–190.

[4] S.W. Min, S.H. Cho, Y. Zhou, S. Schroeder, V. Haroutunian, W.W. Seeley, E. J. Huang, Y. Shen, E. Masliah, C. Mukherjee, D. Meyers, P.A. Cole, M. Ott, L. Gan, Acetylation of tau inhibits its degradation and contributes to tauopathy, Neuron 67 (6) (2010) 953–966.

[5] T. Arakhamia, C.E. Lee, Y. Carlomagno, D.M. Duong, S.R. Kundinger, K. Wang, D. Williams, M. DeTure, D.W. Dickson, C.N. Cook, N.T. Seyfried, L. Petrucelli, A.W. P. Fitzpatrick, Posttranslational Modifications Mediate the Structural Diversity of Tauopathy Strains, Cell 180 (4) (2020) 633–644 e12.

[6] F.X. Cantrelle, A. Loyens, X. Trivelli, O. Reimann, C. Despres, N.S. Gandhi, C.P. R. Hackenberger, I. Landrieu, C. Smet-Nocca, Phosphorylation and O-GlcNAcylation of the PHF-1 Epitope of Tau Protein Induce Local Conformational Changes of the C-Terminus and Modulate Tau Self-Assembly Into Fibrillar Aggregates, Front Mol Neurosci 14 (2021) 661368.

[7] N. Kyalu Ngoie Zola, C. Balty, S. Pyr dit Ruys, A.A.T. Vanparys, N.D.G. Huyghe, G. Herinckx, M. Johanns, E. Boyer, P. Kienlen-Campard, M.H. Rider, D. Vertommen, B.J. Hanseeuw, Specific post-translational modifications of soluble tau protein distinguishes Alzheimer's disease and primary tauopathies Nature Communications 14 1 2023.

[8] Y. Wang, E. Mandelkow, Tau in physiology and pathology, Nat Rev Neurosci 17 (1) (2016) 5–21.

[9] G. Limorenko, H.A. Lashuel, Revisiting the grammar of Tau aggregation and pathology formation: how new insights from brain pathology are shaping how we study and target Tauopathies, Chem Soc Rev 51 (2) (2022) 513–565.

[10] T.J. Cohen, J.L. Guo, D.E. Hurtado, L.K. Kwong, I.P. Mills, J.Q. Trojanowski, V. M. Lee, The acetylation of tau inhibits its function and promotes pathological tau aggregation, Nat Commun 2 (2011) 252.

[11] P. Chakraborty, G. Riviere, A. Hebestreit, A.I. de Opakua, I.M. Vorberg, L. B. Andreas, M. Zweckstetter, Acetylation discriminates disease-specific tau deposition, Nat Commun 14 (1) (2023) 5919.

[12] D. Komander, M. Rape, The ubiquitin code, Annu Rev Biochem 81 (2012) 203–229.

[13] M. Morishima-Kawashima, M. Hasegawa, K. Takio, M. Suzuki, K. Titani, Y. Ihara, Ubiquitin is conjugated with amino-terminally processed tau in paired helical filaments, Neuron 10 (6) (1993) 1151–1160.

[14] L. Petrucelli, D. Dickson, K. Kehoe, J. Taylor, H. Snyder, A. Grover, M. De Lucia, E. McGowan, J. Lewis, G. Prihar, J. Kim, W.H. Dillmann, S.E. Browne, A. Hall, R. Voellmy, Y. Tsuboi, T.M. Dawson, B. Wolozin, J. Hardy, M. Hutton, CHIP and Hsp70 regulate tau ubiquitination, degradation and aggregation, Hum Mol Genet 13 (7) (2004) 703–714.

[15] H. Wesseling, W. Mair, M. Kumar, C.N. Schlaffner, S. Tang, P. Beerepoot, B. Fatou, A.J. Guise, L. Cheng, S. Takeda, J. Muntel, M.S. Rotunno, S. Dujardin, P. Davies, K. S. Kosik, B.L. Miller, S. Berretta, J.C. Hedreen, L.T. Grinberg, W.W. Seeley, B.T. Hyman, H. Steen, J.A. Steen, Tau PTM Profiles Identify Patient Heterogeneity and Stages of Alzheimer's Disease, Cell 183(6) (2020) 1699-1713 e13.

[16] M.H. Abreha, E.B. Dammer, L. Ping, T. Zhang, D.M. Duong, M. Gearing, J.J. Lah, A. I. Levey, N.T. Seyfried, Quantitative Analysis of the Brain Ubiquitylome in Alzheimer's Disease, Proteomics 18 (20) (2018) e1800108.

[17] F. Munari, C.G. Barracchia, C. Franchin, F. Parolini, S. Capaldi, A. Romeo, L. Bubacco, M. Assfalg, G. Arrigoni, M. D'Onofrio, Semisynthetic and Enzyme-Mediated Conjugate Preparations Illuminate the Ubiquitination-Dependent Aggregation of Tau Protein, Angew Chem Int Ed Engl 59 (16) (2020) 6607–6611.

[18] F. Parolini, R. Tira, C.G. Barracchia, F. Munari, S. Capaldi, M. D'Onofrio, M. Assfalg, Ubiquitination of Alzheimer's-related tau protein affects liquid-liquid phase separation in a site- and cofactor-dependent manner, Int J Biol Macromol 201 (2022) 173–181.

[19] F. Parolini, E. Ataie Kachoie, G. Leo, L. Civiero, L. Bubacco, G. Arrigoni, F. Munari, M. Assfalg, M. D'Onofrio, S. Capaldi, Site-Specific Ubiquitination of Tau Amyloids Promoted by the E3 Ligase CHIP, Angew Chem Int Ed Engl 62 (50) (2023) e202310230.

[20] W. Gui, G.A. Davidson, Z. Zhuang, Chemical methods for protein site-specific ubiquitination, RSC Chem Biol 2 (2) (2021) 450–467.

[21] Y. Huppelschoten G.J. van der Heden van Noort, State of the art in (semi-)synthesis of Ubiquitin- and Ubiquitin-like tools Semin Cell Dev Biol 132 2022 74 85.

[22] P.E. Dawson, T.W. Muir, I. Clark-Lewis, S.B. Kent, Synthesis of proteins by native chemical ligation, Science 266 (5186) (1994) 776–779.

[23] C. Chatterjee, R.K. McGinty, J.P. Pellois, T.W. Muir, Auxiliary-mediated site-specific peptide ubiquitylation, Angew Chem Int Ed Engl 46 (16) (2007) 2814–2818.

[24] C.E. Weller, A. Dhall, F. Ding, E. Linares, S.D. Whedon, N.A. Senger, E.L. Tyson, J. D. Bagert, X. Li, O. Augusto, C. Chatterjee, Aromatic thiol-mediated cleavage of N-O bonds enables chemical ubiquitylation of folded proteins, Nat Commun 7 (2016) 12979.

[25] M. Hejjaoui, M. Haj-Yahya, K.S. Kumar, A. Brik, H.A. Lashuel, Towards elucidation of the role of ubiquitination in the pathogenesis of Parkinson's disease with semisynthetic ubiquitinated alpha-synuclein, Angew Chem Int Ed Engl 50 (2) (2011) 405–409.

[26] M. Pan, S. Gao, Y. Zheng, X. Tan, H. Lan, X. Tan, D. Sun, L. Lu, T. Wang, Q. Zheng, Y. Huang, J. Wang, L. Liu, Quasi-Racemic X-ray Structures of K27-Linked Ubiquitin Chains Prepared by Total Chemical Synthesis, J Am Chem Soc 138 (23) (2016) 7429–7435.

[27] C. Castaneda, J. Liu, A. Chaturvedi, U. Nowicka, T.A. Cropp, D. Fushman, Nonenzymatic assembly of natural polyubiquitin chains of any linkage composition and isotopic labeling scheme, J Am Chem Soc 133 (44) (2011) 17855–17868.

[28] S. Virdee, Y. Ye, D.P. Nguyen, D. Komander, J.W. Chin, Engineered diubiquitin synthesis reveals Lys29-isopeptide specificity of an OTU deubiquitinase, Nat Chem Biol 6 (10) (2010) 750–757.

[29] C. Chatterjee, R.K. McGinty, B. Fierz, T.W. Muir, Disulfide-directed histone ubiquitylation reveals plasticity in hDot1L activation, Nat Chem Biol 6 (4) (2010) 267–269.

[30] F. Meier, T. Abeywardana, A. Dhall, N.P. Marotta, J. Varkey, R. Langen, C. Chatterjee, M.R. Pratt, Semisynthetic, site-specific ubiquitin modification of alpha-synuclein reveals differential effects on aggregation, J Am Chem Soc 134 (12) (2012) 5468–5471.

[31] V.H. Trang, E.M. Valkevich, S. Minami, Y.C. Chen, Y. Ge, E.R. Strieter, Nonenzymatic polymerization of ubiquitin: single-step synthesis and isolation of discrete ubiquitin oligomers, Angew Chem Int Ed Engl 51 (52) (2012) 13085–13088.

[32] R. Meledin, S.M. Mali, S.K. Singh, A. Brik, Protein ubiquitination via dehydroalanine: development and insights into the diastereoselective 1,4-addition step, Org Biomol Chem 14 (21) (2016) 4817–4823.

[33] F. Munari, C.G. Barracchia, F. Parolini, R. Tira, L. Bubacco, M. Assfalg, M. D'Onofrio, Semisynthetic Modification of Tau Protein with Di-Ubiquitin Chains for Aggregation Studies, Int J Mol Sci 21 (12) (2020).

[34] D. Trivellato, F. Floriani, C. Giorgio Barracchia, F. Munari, M. D'Onofrio, M. Assfalg, Site-directed double monoubiquitination of the repeat domain of the amyloid-forming protein tau impairs self-assembly and coacervation, Bioorg Chem 132 (2023) 106347.

[35] J. Chen, Y. Ai, J. Wang, L. Haracska, Z. Zhuang, Chemically ubiquitylated PCNA as a probe for eukaryotic translesion DNA synthesis, Nat Chem Biol 6 (4) (2010) 270–272.

[36] J. Dadova, S.R. Galan, B.G. Davis, Synthesis of modified proteins via functionalization of dehydroalanine, Curr Opin Chem Biol 46 (2018) 71–81.

[37] J.M. Chalker, S.B. Gunnoo, O. Boutureira, S.C. Gerstberger, M. Fernández-González, G.J.L. Bernardes, L. Griffin, H. Hailu, C.J. Schofield, B.G. Davis, Methods for converting cysteine to dehydroalanine on peptides and proteins, Chemical Science 2 (9) (2011) 1666–1676.

[38] P.R. Lindstedt, R.J. Taylor, G.J.L. Bernardes, M. Vendruscolo, Facile Installation of Post-translational Modifications on the Tau Protein via Chemical Mutagenesis, Acs Chemical Neuroscience 12 (3) (2021) 557–561.

[39] Z.F. Brotzakis, P.R. Lindstedt, R.J. Taylor, D.J. Rinauro, N.C.T. Gallagher, G.J. L. Bernardes, M. Vendruscolo, A Structural Ensemble of a Tau-Microtubule Complex Reveals Regulatory Tau Phosphorylation and Acetylation Mechanisms, ACS Cent Sci 7 (12) (2021) 1986–1995.

[40] D. Cripps, S.N. Thomas, Y. Jeng, F. Yang, P. Davies, A.J. Yang, Alzheimer disease-specific conformation of hyperphosphorylated paired helical filament-Tau is polyubiquitinated through Lys-48, Lys-11, and Lys-6 ubiquitin conjugation, J Biol Chem 281 (16) (2006) 10825–10838.

[41] T.W. Muir, D. Sondhi, P.A. Cole, Expressed protein ligation: a general method for protein engineering, Proc Natl Acad Sci U S A 95 (12) (1998) 6705–6710.

[42] A.C. Conibear, E.E. Watson, R.J. Payne, C.F.W. Becker, Native chemical ligation in protein synthesis and semi-synthesis, Chem Soc Rev 47 (24) (2018) 9046–9068.

[43] L. De Rosa, R. Di Stasi, L.D. D'Andrea, Total chemical synthesis by native chemical ligation of the all-D immunoglobulin-like domain 2 of Axl, Tetrahedron 75 (7) (2019) 894–905.

[44] M.D. Mukrasch, S. Bibow, J. Korukottu, S. Jeganathan, J. Biernat, C. Griesinger, E. Mandelkow, M. Zweckstetter, Structural polymorphism of 441-residue tau at single residue resolution, PLoS Biol 7 (2) (2009) e34.

[45] F. Munari, M. D'Onofrio, M. Assfalg, Solution NMR insights into dynamic supramolecular assemblies of disordered amyloidogenic proteins, Arch Biochem Biophys 683 (2020) 108304.

[46] D.P. Vogl, A.C. Conibear, C.F.W. Becker, Segmental and site-specific isotope labelling strategies for structural analysis of posttranslationally modified proteins, RSC Chem Biol 2 (5) (2021) 1441–1461.

[47] R. Varadan, M. Assfalg, D. Fushman, Using NMR spectroscopy to monitor ubiquitin chain conformation and interactions with ubiquitin-binding domains, Methods Enzymol 399 (2005) 177–192.

[48] M. Biancalana, S. Koide, Molecular mechanism of Thioflavin-T binding to amyloid fibrils, Biochim Biophys Acta 1804 (7) (2010) 1405–1412.

[49] C.G. Barracchia, R. Tira, F. Parolini, F. Munari, L. Bubacco, G.A. Spyroulias, M. D'Onofrio, M. Assfalg, Unsaturated Fatty Acid-Induced Conformational Transitions and Aggregation of the Repeat Domain of Tau, Molecules 25 (11) (2020).

[50] D. Ellmer, M. Brehs, M. Haj-Yahya, H.A. Lashuel, C.F.W. Becker, Single Posttranslational Modifications in the Central Repeat Domains of Tau4 Impact its Aggregation and Tubulin Binding, Angew Chem Int Ed Engl 58 (6) (2019) 1616–1620.

[51] A. Jangholi, M.R. Ashrafi-Kooshk, S.S. Arab, G. Riazi, F. Mokhtari, M. Poorebrahim, H. Mahdiuni, B.I. Kurganov, A.A. Moosavi-Movahedi, R. Khodarahmi, Appraisal of role of the polyanionic inducer length on amyloid formation by 412-residue 1N4R Tau protein: A comparative study, Arch Biochem Biophys 609 (2016) 1–19.

[52] S. Ojaghi, S. Mohammadi, M. Amani, S. Ghobadi, N. Bijari, S. Esmaeili, R. Khodarahmi, Sunset yellow degradation product, as an efficient water-soluble inducer, accelerates 1N4R Tau amyloid oligomerization: In vitro preliminary evidence against the food colorant safety in terms of "Triggered Amyloid Aggregation", Bioorg Chem 103 (2020) 104123.

[53] S. Sundararaj, A. Guo, B. Habibi-Nazhad, M. Rouani, P. Stothard, M. Ellison, D.S. Wishart, The CyberCell Database (CCDB): a comprehensive, self-updating, relational database to coordinate and facilitate in silico modeling of Escherichia coli, Nucleic Acids Res 32(Database issue) (2004) D293-5.
[54] F.X. Theillet, A. Binolfi, T. Frembgen-Kesner, K. Hingorani, M. Sarkar, C. Kyne, C. Li, P.B. Crowley, L. Gierasch, G.J. Pielak, A.H. Elcock, A. Gershenson, P. Selenko, Physicochemical properties of cells and their effects on intrinsically disordered proteins (IDPs), Chem Rev 114 (13) (2014) 6661–6714.
[55] N. Psychogios, D.D. Hau, J. Peng, A.C. Guo, R. Mandal, S. Bouatra, I. Sinelnikov, R. Krishnamurthy, R. Eisner, B. Gautam, N. Young, J. Xia, C. Knox, E. Dong, P. Huang, Z. Hollander, T.L. Pedersen, S.R. Smith, F. Bamforth, R. Greiner, B. McManus, J.W. Newman, T. Goodfriend, D.S. Wishart, The human serum metabolome, PLoS One 6 (2) (2011) e16957.
[56] S.A. Bradley, A. Ouyang, J. Purdie, T.A. Smitka, T. Wang, A. Kaerner, Fermentanomics: monitoring mammalian cell cultures with NMR spectroscopy, J Am Chem Soc 132 (28) (2010) 9531–9533.
[57] T. Geiger, A. Wehner, C. Schaab, J. Cox, M. Mann, Comparative proteomic analysis of eleven common cell lines reveals ubiquitous but varying expression of most proteins, Mol Cell Proteomics 11 (3) (2012) M111–014050.
[58] G.G. Kovacs, I. Ferrer, L.T. Grinberg, I. Alafuzoff, J. Attems, H. Budka, N.J. Cairns, J.F. Crary, C. Duyckaerts, B. Ghetti, G.M. Halliday, J.W. Ironside, S. Love, I. R. Mackenzie, D.G. Munoz, M.E. Murray, P.T. Nelson, H. Takahashi, J. Q. Trojanowski, O. Ansorge, T. Arzberger, A. Baborie, T.G. Beach, K.F. Bieniek, E. H. Bigio, I. Bodi, B.N. Dugger, M. Feany, E. Gelpi, S.M. Gentleman, G. Giaccone, K. J. Hatanpaa, R. Heale, P.R. Hof, M. Hofer, T. Hortobagyi, K. Jellinger, G.A. Jicha, P. Ince, J. Kofler, E. Kovari, J.J. Kril, D.M. Mann, R. Matej, A.C. McKee, C. McLean, I. Milenkovic, T.J. Montine, S. Murayama, E.B. Lee, J. Rahimi, R.D. Rodriguez, A. Rozemuller, J.A. Schneider, C. Schultz, W. Seeley, D. Seilhean, C. Smith, F. Tagliavini, M. Takao, D.R. Thal, J.B. Toledo, M. Tolnay, J.C. Troncoso, H. V. Vinters, S. Weis, S.B. Wharton, C.L. White 3rd, T. Wisniewski, J.M. Woulfe, M. Yamada, D.W. Dickson, Aging-related tau astrogliopathy (ARTAG): harmonized evaluation strategy, Acta Neuropathol 131 (1) (2016) 87–102.
[59] T. Mothes, B. Portal, E. Konstantinidis, K. Eltom, S. Libard, L. Streubel-Gallasch, M. Ingelsson, J. Rostami, M. Lindskog, A. Erlandsson, Astrocytic uptake of neuronal corpses promotes cell-to-cell spreading of tau pathology, Acta Neuropathol Commun 11 (1) (2023) 97.
[60] S. Oddo, A. Caccamo, J.D. Shepherd, M.P. Murphy, T.E. Golde, R. Kayed, R. Metherate, M.P. Mattson, Y. Akbari, F.M. LaFerla, Triple-transgenic model of Alzheimer's disease with plaques and tangles: intracellular Abeta and synaptic dysfunction, Neuron 39 (3) (2003) 409–421.
[61] C. Vianello, M. Salluzzo, D. Anni, D. Boriero, M. Buffelli, L. Carboni, Increased Expression of Autophagy-Related Genes in Alzheimer's Disease-Type 2 Diabetes Mellitus Comorbidity Models in Cells, Int J Environ Res Public Health 20 (5) (2023).
[62] J.R. Perea, E. Lopez, J.C. Diez-Ballesteros, J. Avila, F. Hernandez, M. Bolos, Extracellular Monomeric Tau Is Internalized by Astrocytes, Front Neurosci 13 (2019) 442.
[63] R. Varadan, M. Assfalg, S. Raasi, C. Pickart, D. Fushman, Structural determinants for selective recognition of a Lys48-linked polyubiquitin chain by a UBA domain, Mol Cell 18 (6) (2005) 687–698.